Highly Structured Water Networks in Microhydrated Dodecaborate Clusters

Journal:	*The Journal of Physical Chemistry Letters*
Manuscript ID	jz-2022-03077h
Manuscript Type:	Letter
Date Submitted by the Author:	10-Oct-2022
Complete List of Authors:	Jiang, Yanrong; East China Normal University Cai, Zhaojie; East China Normal University Yuan, Qinqin; Pacific Northwest National Laboratory Cao, Wenjin; Pacific Northwest National Laboratory, Physical Sciences Division Hu, Zhubin; East China Normal University, State Key Laboratory of Precision Spectroscopy Sun, Haitao; State Key Laboratory of Precision Spectroscopy, Department of Physics Wang, Xue-Bin; Pacific Northwest National Laboratory, Chemical & Materials Scienecs Division Sun, Zhenrong; East China Normal University, Department of Physics

Highly Structured Water Networks in Microhydrated Dodecaborate Clusters

Yanrong Jiang[1,3#], Zhaojie Cai[1#], Qinqin Yuan[2], Wenjin Cao[2], Zhubin Hu[1], Haitao Sun[1,4,5*], Xue-Bin Wang[2*] and Zhenrong Sun[1,4*]

[1] *State Key Laboratory of Precision Spectroscopy, School of Physics and Electronic Science, East China Normal University, Shanghai 200241, China*

[2] *Physical Sciences Division, Pacific Northwest National Laboratory, 902 Battelle Boulevard, P.O. Box 999, Richland, Washington 99352, USA*

[3] *Center for Transformative Science, ShanghaiTech University, Shanghai 201210, China*

[4] *Collaborative Innovation Center of Extreme Optics, Shanxi University, Taiyuan, Shanxi 030006, China*

[5] *NYU-ECNU Center for Computational Chemistry at NYU Shanghai, Shanghai, 200062, China*

[#]Y. Jiang and Z. Cai contributed equally to this work.

*Corresponding author: htsun@phy.ecnu.edu.cn (H.S.); xuebin.wang@pnnl.gov (X.-B.W.) and zrsun@phy.ecnu.edu.cn (Z. R. S.).

ABSTRACT: We report a combined negative ion photoelectron spectroscopy and theoretical investigation on a series of size-selected hydrated *closo*-dodecaborate clusters $B_{12}X_{12}^{2-}\cdot nH_2O$ (X = H, F, I; n = 1 – 6). Distinct structural arrangements of water clusters from monomer to hexamer can be achieved by using different $B_{12}X_{12}^{2-}$ bases (X = H, F, I), illustrating evident solute specificity. Due to the superior strength of B-H···H-O dihydrogen bonds (solute – solvent) versus conventional O···H-O hydrogen bonds in water (solvent – solvent), the added water molecules are arranged in a unified binding mode by forming highly structured water networks manipulated by $B_{12}H_{12}^{2-}$. As a comparison, the hydrated $B_{12}F_{12}^{2-}$ clusters display similar water evolution patterns for monomer and dimer, but different binding modes for larger clusters, while the hydrated $B_{12}I_{12}^{2-}$ share similarities with the free water clusters. The present finding provides a consistent picture of the structural diversity of the hydrogen-bonding networks in the microhydrated dodecaborate clusters, and a molecular-level understanding of the microsolvation dynamics in aqueous borate chemistry.

TOC Graphic

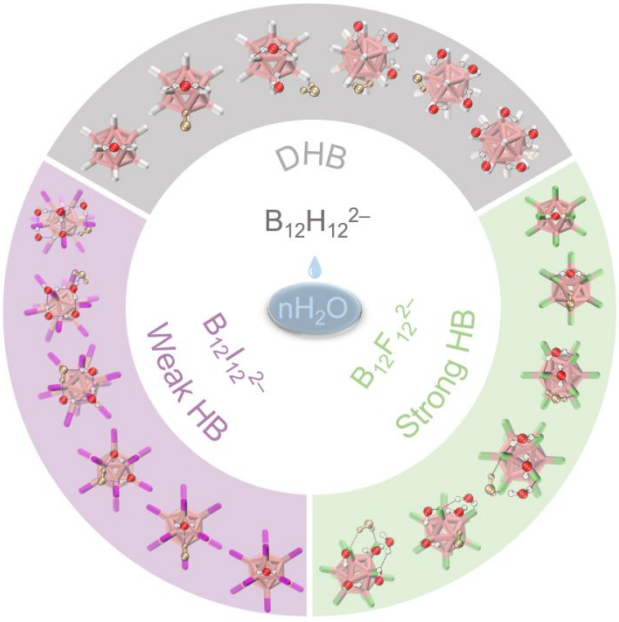

Ion−water interaction in aqueous solution remains one of the most interesting and highly debated topics throughout biology, chemistry, atmosphere, and materials science[1-5]. For example, ion hydration is not only crucial for the conformations and activities of biomolecules such as membranes, enzymes, and drugs[6-8], but also significantly affects the rates of chemical reactions and separations.[9-10] The nature of ion−water interactions is often described in terms of the structure maker/"kosmotropes" or breaker/"chaotropes" concept,[11-12] which can be related to the well-known macroscopically observed Hofmeister series.[13-14] In particular, it is now believed that solute specific effects[2, 15-16] through the insertion of the solute ions either enhance or disrupt the water hydrogen-bonding (HB) network according to its internal geometry and charge distribution. This behavior also accounts for many of the physicochemical and thermochemical properties of the associated solvation processes, including vapor–liquid interface effect,[17] the entropic signature of the hydrophobic effect,[18-19] and the associated enthalpic signatures.[11] Thus, a molecular-level understanding of the microstructure of ionic water clusters and its evolution of HB networks remains a grand challenge.[15, 20-29]

Notably, the *closo*-dodecaborate $B_{12}H_{12}^{2-}$ and related halogenated derivatives $B_{12}X_{12}^{2-}$ (X = F–I) were classified as superchaotropic ions[19] beyond the traditional Hoffmeister scale. The delocalized three-center/two-electron bonding pattern of $B_{12}H_{12}^{2-}$ making two excess negative charges stabilized in a delocalized σ-electron system renders a specific charge distribution, and high electronic and thermodynamic stability.[30] And the behavior of charge distribution can be inversely tuned through substitution of various halogen shells.[31] Very recently, those dodecaborate clusters have been demonstrated as excellent anionic inorganic carriers for membrane translocation of hydrophilic substances[6], promising candidates in supramolecular encapsulation for boron neutron capture therapy application[32-33] and specific and potent inhibitors of HIV protease inhibitors.[34] Peculiar organization of the water molecules in the first solvation shell of $B_{12}H_{12}^{2-}$ was observed with the formation of a dihydrogen bond (DHB) of B-H···H-O between the hydrogen atoms of the anions and the hydrogen atoms of the water

molecules by molecular dynamics (MD) simulation.[35] A recent study by us has also demonstrated such a hydridic-to-protonic DHB predominance based on the monohydrated *closo*-dodecaborate cluster $B_{12}H_{12}^{2-}\cdot H_2O$ compared with its halogenated derivatives.[36] However, the nature of the interaction of these dodecaborate clusters with biological interfaces in aqueous environments has not yet been understood. In particular, the knowledge of how ion−water interactions behave from the gas phase to bulk has remained unclear. The influence of incremental hydration of the dodecaborate dianions and how the predominant DHBs affect the structural evolution of the H-bond networks in the first water shell remains an open question.

Here we report a systematic investigation on the electronic structures and intermolecular interactions of a series of size-selected hydrated *closo*-dodecaborate clusters $B_{12}X_{12}^{2-}\cdot nH_2O$ (X = H, F, I; *n* = 1–6) through combining negative ion photoelectron spectroscopy and quantum chemical calculations. Due to the subtle competition existing between B-X···H-O (solute-solvent) and O-H···O (solvent-solvent) in water clusters, this series of hydrated clusters with stepwise increases of water molecules represents an ingenious model to examine various water cluster growth patterns under the control of different $B_{12}X_{12}^{2-}$. Structural optimizations and dynamic simulations on the whole series of the hydrated clusters reveal that attached water clusters can be manipulated in an orderly arrangement by $B_{12}H_{12}^{2-}$ due to the existence of the unique superior B-H···H-O DHBs.

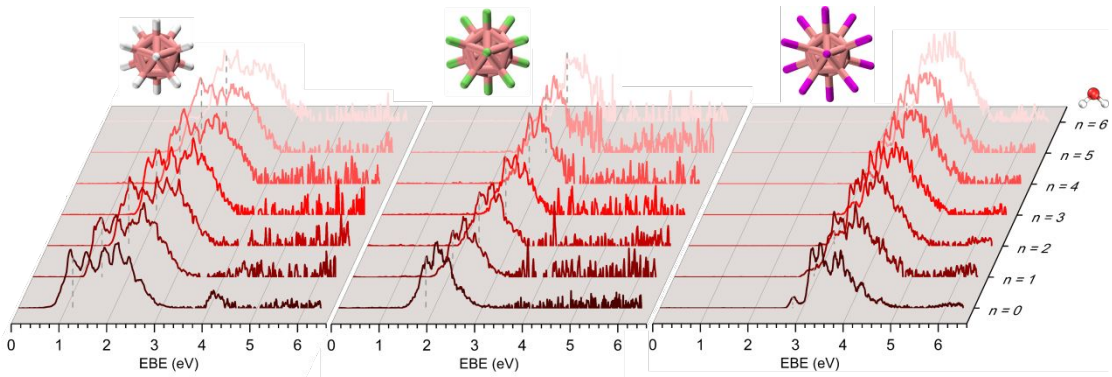

Figure 1. The 20K NIPE spectra of $B_{12}X_{12}^{2-}\cdot nH_2O$ (X = H, F, I; n = 0–6) measured with 193 nm photons. The dashed gray lines designate the spectral VDEs position. The noisy spikes in the spectrum of the hydrated F series beyond 4 eV are due to imperfect

background subtraction originated from weak signals and scaled down by a factor of 0.3 to enhance the presentation clarity. The detailed each individual spectrum is given in Figure S1(a). Boron, hydrogen, oxygen, fluorine, and iodine atoms are severally colored in pink, grey, red, green, and magenta. The NIPE spectra of $B_{12}X_{12}^{2-}\cdot H_2O$ (X = H, F, I) were taken from reference [36].

Table 1 Experimental VDEs (eV) and ΔVDEs (kcal/mol) in comparison to calculated VDEs (eV) at DLPNO-CCSD(T)/aug-cc-pVTZ(-pp) level and binding energies (BEs, in kcal/mol) at SAPT2+/aug-cc-pVDZ(-pp) level for $B_{12}X_{12}^{2-}\cdot nH_2O$ (X = H, F, I; n = 1–6).

	$B_{12}H_{12}^{2}$				$B_{12}F_{12}^{2}$				$B_{12}I_{12}^{2}$			
	VDE		ΔVDE[a]	BE	VDE		ΔVDE[a]	BE	VDE		ΔVDE[a]	BE
	Expt.	Cal.	Expt.	Cal.	Expt.	Cal.	Expt.	Cal.	Expt.	Cal.	Expt.	Cal.
Isolated	1.15	1.36	-	-	1.85	2.07	-	-	2.80	2.86	-	-
$1H_2O$	1.46	1.70	7.15 (0.31)	14.31	2.11	2.34	6.00 (0.26)	13.16	2.91	3.05	2.54 (0.11)	8.74
$2H_2O$	1.73	1.95	13.38 (0.58)	26.64	2.36	2.56	11.76 (0.51)	23.97	3.09	3.17	6.69 (0.29)	16.60
$3H_2O$	1.97	2.18	18.91 (0.82)	37.83	2.60	2.78	17.30 (0.75)	34.93	3.19	3.23	8.99 (0.39)	20.78
$4H_2O$	2.19	2.42	23.98 (1.04)	47.88	2.80	3.01	21.91 (0.95)	44.69	3.24	3.27	10.15 (0.44)	23.41
$5H_2O$	2.31	2.53	26.75 (1.16)	53.16	2.83	3.01	22.60 (0.98)	44.97	3.34	3.50	12.45 (0.54)	30.63
$6H_2O$	2.53	2.80	31.82 (1.38)	65.73	2.98	3.18	26.06 (1.13)	54.08	3.36	3.46	12.91 (0.56)	35.12

[a]ΔVDE was experimentally determined as VDE difference between $B_{12}X_{12}^{2-}\cdot nH_2O$ and isolated $B_{12}X_{12}^{2-}$, i.e., VDE ($B_{12}X_{12}^{2-}\cdot nH_2O$) – VDE ($B_{12}X_{12}^{2-}$) = [E($B_{12}X_{12}^{2-}\cdot nH_2O$) – E($B_{12}X_{12}^{2-}$)] – [E($B_{12}X_{12}^{\bullet-}\cdot nH_2O$) – E($B_{12}X_{12}^{\bullet-}$)], and values in parentheses are in eV. The NIPES data of $B_{12}X_{12}^{2-}\cdot H_2O$ (X = H, F, I) were taken from reference [36].

Figure 1 shows the 20 K NIPE spectra of $B_{12}X_{12}^{2-}\cdot nH_2O$ (X = H, F, I; n = 0 − 6). First, the spectral shapes of hydrated $B_{12}X_{12}^{2-}\cdot nH_2O$ (n = 1 − 6) resemble similar patterns compared to each corresponding isolated $B_{12}X_{12}^{2-}$, with their electron binding energies (EBEs) blue shifted upon H_2O additions. Due to the existence of repulsive Coulomb barrier in photodetaching dianions, spectral bands at higher binding energy

are suppressed and see Figure S1(b) for comparing 193 and 157 nm spectra of $B_{12}H_{12}^{2-}\cdot nH_2O$. The $B_{12}H_{12}^{2-}$ with the smallest vertical detachment energy (VDE) among the three $B_{12}X_{12}^{2-}$ anions exhibits a significant VDE shift of 0.31 eV when one H_2O molecule is attached, followed by shifts of 0.27, 0.24, and 0.22 eV, respectively, with the additions of the 2nd, 3rd, and 4th H_2O molecules (Table 1). Then only a slightly smaller VDE shift of 0.12 eV is seen for n = 5, followed by a larger shift of 0.22 eV for n = 6. The VDE shifts for $B_{12}F_{12}^{2-}\cdot nH_2O$ clusters are measured to be 0.26, 0.25, 0.24, 0.20, 0.03, and 0.15 eV for n = 1 – 6, respectively, which are slightly smaller compared to those of $B_{12}H_{12}^{2-}\cdot nH_2O$ and similarly exhibit a "plateau" at n = 5. Different from these two clusters, the $B_{12}I_{12}^{2-}\cdot nH_2O$ clusters have much smaller VDE shifts upon hydration and do not show a "plateau" at n = 5 neither (Table 1 and Figure 2). The measured NIPE spectra here provides crucial information in determining the structures of these clusters when combining with theoretical calculations. Thus, the structural evolution of lowest-lying hydrated clusters (Figure 3) and corresponding VDEs (Table 1) were computationally located. Three theoretical methods in different levels including DLPNO-CCSD(T), IP-EOM-DLPNO-CCSD, and PBE0 were employed to calculate the VDEs by comparing with the experimental data (Figure 2). Overall the DLPNO-CCSD(T) and IP-EOM-DLPNO-CCSD methods are found to well reproduce the experimental measurements qualitatively and quantitatively, while PBE0 fails to give quantitative predictions for I series. In addition, the structures and corresponding VDEs of three low-lying isomers were also presented in Figure S2 and Table S2. The small differences of relative energies and similarity of VDEs indicate that these low-lying isomers may coexist in the experiments and contribute to a relatively lower spectral resolution of the measured NIPE spectra (Figure S1).

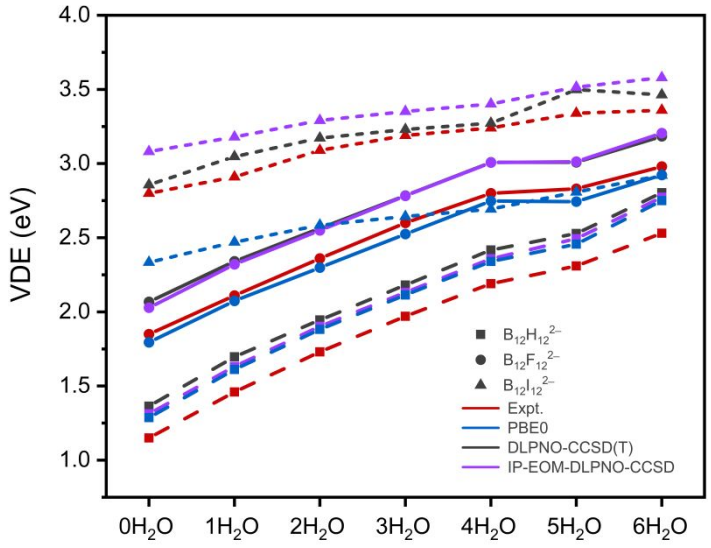

Figure 2. Experimental VDEs and calculated VDEs of $B_{12}X_{12}^{2-}\cdot nH_2O$ (X = H, F, I; n = 0–6) using DLPNO-CCSD(T) (in black), IP-EOM-DLPNO-CCSD (in purple), and PBE0 (in blue) methods with the aug-cc-pVTZ(-pp) basis set.

For $B_{12}H_{12}^{2-}\cdot H_2O$, the two hydrogens of the 1st water point to the two adjacent $H^{\delta-}$–B bonds to form double DHBs as previously revealed.[36] For n = 2, one H atom of the 2nd water interacts with a third $H^{\delta-}$–B bond that forms an equilateral triangle with the first two $H^{\delta-}$–B bonds linked to the 1st water, while the other hydrogen atom hydrogen bonded to the oxygen atom of the initial water. Interestingly, the isomers with 2nd water binding at the symmetrical opposite sites by forming four DHBs (Figure S2g) locate less stable. This can be explained by the fact that the most stable configuration possesses a shortened DHB length of 1.76 Å versus normal DHB lengths of 1.83-1.84 Å and the binding strength can be obviously enhanced. The third water continues the previous binding mode without breaking the original binding configuration in $B_{12}H_{12}^{2-}\cdot 2H_2O$. Such a binding motif continues for n = 4 and 5. Therefore the water growth pattern from n = 1 to 5 vividly illustrates that the $B_{12}H_{12}^{2-}$ solute can manipulate water molecules in an orderly queue with a uniform binding motif, due to the superior strength of B-H···H-O DHBs versus typical O···H-O HBs in water clusters. Especially for $B_{12}H_{12}^{2-}\cdot 5H_2O$, water pentamer displays an almost coplanar regular five-membered ring, in which one H atom of each water points to one H node of $B_{12}H_{12}^{2-}$ to form a

DHB, while the other H binds to the oxygen atom of an adjacent water to form O···H-O HB. Interestingly, such a cyclic water pentamer was also observed in the hydration of biomolecular systems, i.e., protein crambin[37] and of a deoxydinucleoside–drug complex[38] through X-ray diffraction analysis. Notably, for $B_{12}H_{12}^{2-}\cdot 6H_2O$, the added water molecule tends to bind to the opposite side with respect to the original $B_{12}H_{12}^{2-}\cdot 5H_2O$ by preferentially forming a new double DHB.

The hydrated $B_{12}F_{12}^{2-}$ clusters display similar water evolution patterns as $B_{12}H_{12}^{2-}\cdot nH_2O$ for n = 1 and 2. However, starting from n = 3, a different binding mode is observed, i.e., there is always one water molecule in the 2nd solvation shell without directly contacting the $B_{12}F_{12}^{2-}$ base. In contrast to being a planar five-membered ring for the water pentamer in $B_{12}H_{12}^{2-}\cdot 5H_2O$, the five water molecules in $B_{12}F_{12}^{2-}\cdot 5H_2O$ display a stereoscopic configuration; while the corresponding isomer with a planar five-membered ring possesses a relatively higher energy of 0.898 kcal/mol (Figure S2). And the water hexamer in $B_{12}F_{12}^{2-}\cdot 6H_2O$ shows an irregular cubic structure.

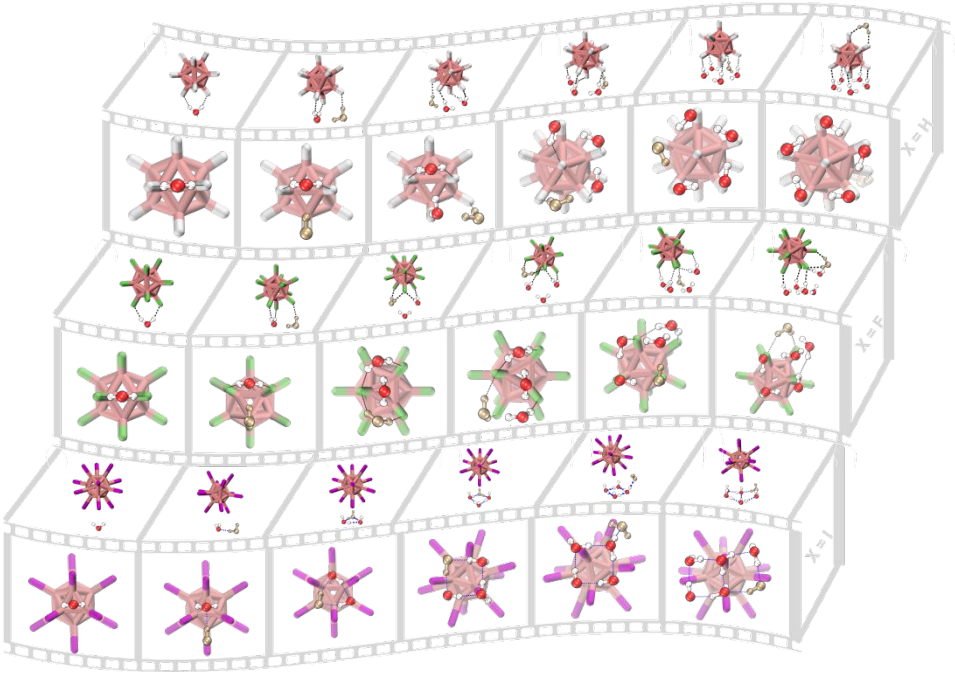

Figure 3. Structural evolution of water clusters from monomer to hexamer under the control of $B_{12}X_{12}^{2-}$ (X = H, F, I) with both top and side views. The bonding networks of B-X···H-O in $B_{12}X_{12}^{2-}\cdot nH_2O$ (X = H, F) and O···H-O bond in $B_{12}I_{12}^{2-}\cdot nH_2O$ are

labeled in black and blue dashed lines, respectively. The newly added n^{th} water molecule in $B_{12}X_{12}^{2-}\cdot nH_2O$ ($n \geq 2$) is presented in color gold.

Distinctly different from hydrated $B_{12}H_{12}^{2-}$ and $B_{12}F_{12}^{2-}$ clusters that have shown specific water cluster networks manipulated by their $B_{12}X_{12}^{2-}$ anions, $B_{12}I_{12}^{2-}\cdot nH_2O$ features solvated structures in which the $B_{12}I_{12}^{2-}$ anion only weakly interacts with the water clusters without significantly perturbating their own binding patterns. For instance, for the n = 3 and 4 clusters, they tend to have the $B_{12}I_{12}^{2-}$ anion bound to cyclic water trimer and tetramer, both being predicted as the most stable structures for free $(H_2O)_3$ and $(H_2O)_4$ clusters[23] (Figure S2). For $B_{12}I_{12}^{2-}\cdot 5H_2O$, noncyclic pentamer with a 3D topological configuration is observed in the most stable structure, echoing with the recent study of Yang *et al*. that the low-lying 3D structure for the free water pentamer can coexist with the lowest-energy cyclic isomer[23]. Additionally, the most stable isomer of $B_{12}I_{12}^{2-}\cdot 6H_2O$ possesses a water cluster structure that shares similarity with the most stable planar structure of the free $(H_2O)_6$ cluster.

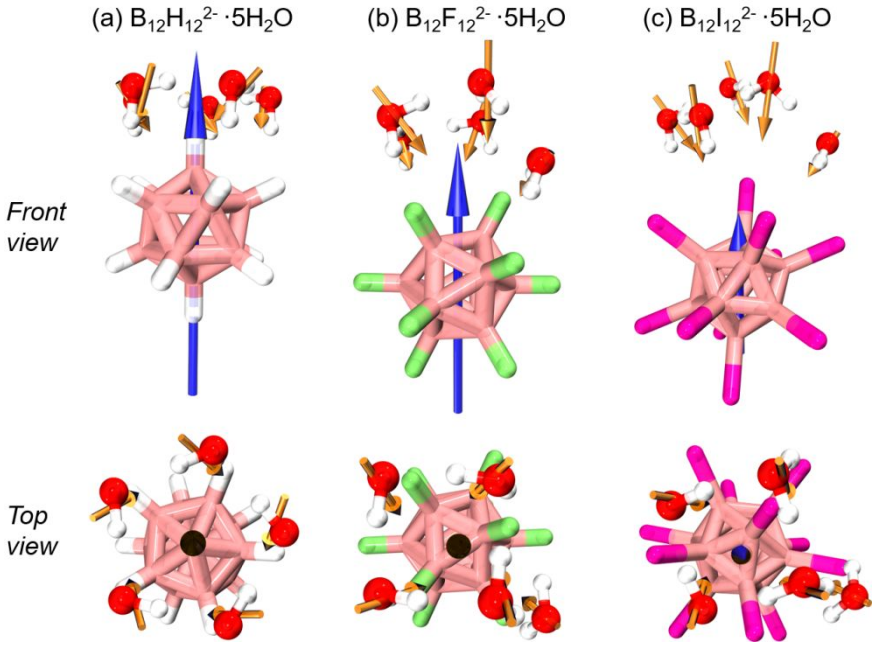

Figure 4. The schematic diagram of decomposed fragment dipole moments for isolated $B_{12}X_{12}^{2-}$ (X = H, F, I) and five water molecules. The blue and yellow arrows represent the dipole moment of fragment of $B_{12}X_{12}^{2-}$ and water molecule, respectively.

In addition, we take the $B_{12}X_{12}^{2-}\cdot 5H_2O$ (X = H, F, I) clusters as a representative model to study the effect of different $B_{12}X_{12}^{2-}$ bases on the orientation of each surrounding water molecule. Thus the decomposed fragment dipole moments and the resulting included angles (θ) between those of isolated $B_{12}X_{12}^{2-}$ and each water molecule were calculated as shown in Figure 4 and Table S3. The orientation of water molecules is found to strongly depend on the specific $B_{12}X_{12}^{2-}$ bases. The negligible value of standard deviation of θ indicates a highly structured water network formed in hydrated $B_{12}H_{12}^{2-}\cdot 5H_2O$, while a less structured water network with more freedom is observed for $B_{12}F_{12}^{2-}\cdot 5H_2O$ and $B_{12}I_{12}^{2-}\cdot 5H_2O$. Interestingly, attaching five water molecules on $B_{12}X_{12}^{2-}$ bases can induce additional dipole moment of different magnitudes for $B_{12}H_{12}^{2-}$ (5.55), $B_{12}F_{12}^{2-}$ (4.55), and $B_{12}I_{12}^{2-}$ (2.78), since the nonattached isolated $B_{12}X_{12}^{2-}$ bases possess no dipole due to their high icosahedral (I_h) symmetry.

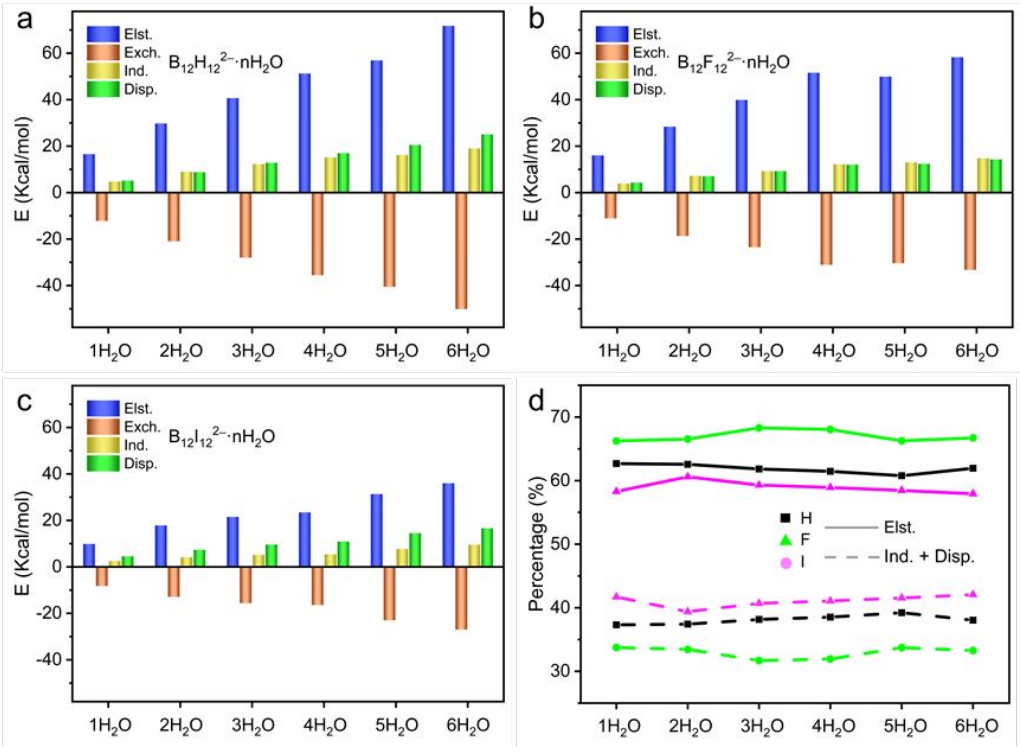

Figure 5. (a, b, c) Electrostatic (Elst.), exchange (Exch.), induction (Ind.), and dispersion (Disp.) terms (kcal/mol) derived from energy decomposition analysis for

$B_{12}X_{12}^{2-}\cdot nH_2O$ (X = H, F, I; n = 1 – 6) at the SAPT2+/aug-cc-pVDZ(-pp) level. (d) Percentages (in %) of the attractive parts, i.e. electrostatic (E_{Elst}) term (in solid line), the sum of induction (E_{Ind}) and dispersion (E_{disp}) terms (in dotted line) contributed to the total attraction.

The above differences of water growth pathways observed in hydrated dodecaborate clusters can be traced back to the competition between solute – solvent and solvent – solvent interactions. First, the numbers of the formed B-X···H-O bonds and O···H-O bonds within these hydrated clusters are checked (Figure S3). For $B_{12}H_{12}^{2-}\cdot nH_2O$ (n = 1 – 6), it possesses 2, 3, 4, 5, 5, 7 B-H···H-O bonds, respectively, colored in dash black in Figure 3, and 0, 1, 2, 3, 5, 5 O···H-O bonds. In comparison, the hydrated $B_{12}F_{12}^{2-}$ clusters hold 2, 3, 4, 5, 5, 6 B-F···H-O and 0, 1, 2, 3, 5, 6 O···H-O bonds for n = 1 – 6, respectively. As a result, the electronic stabilization is found to be particularly related to the number of intermolecular B-X···H-O HBs formed in the clusters and herein such a "plateau" also exists at n = 5 as observed for VDE shifts.

Next, the experimental ΔVDE — the VDE difference between a hydrated complex and corresponding isolated fragments, can be regarded as a direct measurement of their intrinsic binding energy (BE)[39-40]. As shown in Table 1, among three $B_{12}X_{12}^{2-}$ investigated here, the total interaction energy of $B_{12}X_{12}^{2-}$ with water is X = H > F >> I. The calculated total BEs by energy decomposition analysis at SAPT2+/aug-cc-pVDZ(-pp) level well reproduce the experimental trends of ΔVDE (Table S4). Further, the total BEs were decomposed into four physically meaningful components, including electrostatic (Elst.), exchange (Exch.), induction (Ind.), and dispersion (Disp.) terms (Figure 5). The larger BEs in the $B_{12}H_{12}^{2-}\cdot nH_2O$ series arise from their larger electrostatic, induction and dispersion contributions compared to those of $B_{12}F_{12}^{2-}\cdot nH_2O$ and $B_{12}I_{12}^{2-}\cdot nH_2O$. Although the electrostatic interaction is found to still play a dominant role, the induction and dispersion interactions make increasing appreciable contributions, particularly as the water cluster size increases. As shown in Figure 5d and Table S5, the averaged contribution of induction plus dispersion terms to the total attraction for the H series achieves 38%, which is larger than that of 33%

for the F series due to the large polarization effect for the former. The induction plus dispersion contribution reaches to 41% for the I series, which can be attributed to their relatively smaller electrostatic contributions combined with their larger polarizabilities. The results are also confirmed by the noncovalent interaction analysis based on independent gradient model (IGM), where considerable green areas in H series suggesting the more contributions from van der Waals interactions (Figure S4).

In summary, a series of hydrated *closo*-dodecaborate dianion $B_{12}X_{12}^{2-}\cdot nH_2O$ (X = H, F, I; n = 1–6) have been investigated by combining experimental NIPES and multiscale theoretical simulations. The VDEs determined by NIPES measurements agree well with the theoretical predictions. The strength advantage of B-H···H-O DHBs over strong B-F···H-O HBs still holds even disturbed by the competition of solvent – solvent. Furthermore, the structural evolution of water clusters from monomer to hexamer reveals that water cluster growth patterns can be finely manipulated by various $B_{12}X_{12}^{2-}$ due to the subtle competition between B-X···H-O (solute – solvent) and O···H-O (solvent – solvent) HBs. Water monomer to hexamer can be arranged with a uniform binding mode in $B_{12}H_{12}^{2-}\cdot nH_2O$, as a result of the existence of superior B-H···H-O DHBs. The present finding provides an interesting and consistent picture for the structural diversity of the hydrogen-bonding networks in the microhydrated dodecaborate clusters, and a molecular-level understanding of different chemical reactivity and solvation dynamics in aqueous borate chemistry. Moreover, the structural coding of water clusters through the unique dihydrogen interaction of ion – water is worth looking forward to in the future.

Methodology

NIPE spectra measurement. The experiment was carried out using a magnetic-bottle NIPES apparatus equipped with an electrospray ionization source (ESI), a quadruple mass spectrometer, a temperature-controlled cryogenic ion trap and a time-of-flight (TOF) spectrometer[41]. Desired hydrated anion clusters with different sizes $B_{12}X_{12}^{2-}\cdot nH_2O$ (X = H, F, I, n = 1–6) were generated from the ESI source, cooled by collisions with a cold buffer gas (20% H_2 balanced in He) to the cryogenic temperature

of 20K, and then mass-selected to be photodetached by 193 nm photons (6.424 eV, from an ArF laser) or 157 nm photons (7.866 eV) in the interaction zone of the magnetic-bottle photoelectron analyzer. The energy resolution ($\Delta E/E$) was about 2%, i.e., ~20 meV full width at half maximum (FWHM) for 1 eV kinetic energy electrons. Electron binding energies (EBEs) were obtained by subtracting the electron kinetic energies from the detachment photon energy. More experimental details can be found elsewhere[31,36].

Quantum chemical calculation. A systematic procedure of optimization was carried out to obtain the global minimum and low-lying isomers of $B_{12}X_{12}^{2-}\cdot nH_2O$ (X = H, F, I, n = 1–6). First, 50000 initial structures were generated by Molclus code[42], and then optimized and screened efficiently by semi-empirical method of GFN2-xTB[43-44] and PBE0[45]/def2SVP[46]. An energetically sorting for rational structures was performed at the PBE0/TZVP[46] level and re-optimized at the PBE0/aug-cc-pVTZ(-pp)[47-48] level with Grimme's dispersion corrections[49-50]. Finally, the 20K Gibbs free energy was comprised by electronic energy at the DLPNO-CCSD(T)[51-52]/aug-cc-pVTZ(-pp) level using ORCA 5.0.1 codes[53] and thermal correction energy at the PBE0/aug-cc-pVTZ(-pp) level to establish the most stable structure and related isomers without imaginary frequencies (Figure S2). The scaled factor for zero-point energy were set as 0.9771[54]. The calculated vertical detachment energies (VDEs) were obtained by the energy differences between the corresponding monoanions and dianions based on the dianions' optimized geometries. The energy decomposition analysis was performed by the symmetry adapted perturbation theory (SAPT) at the SAPT2+[55-56]/aug-cc-pVDZ(-pp) level using PSI4 code[57]. Independent gradient model (IGM) plots were generated by the Multiwfn code and rendered by the VMD program. All DFT calculations were carried out using the Gaussian 16[58] software.

ASSOCIATED CONTENTS

Supporting Information

Calculated VDEs using the PBE0, DLPNO-CCSD(T), and IP-EOM-DLPNO-CCSD methods; Energy decomposition analysis (EDA) of different components for $B_{12}X_{12}^{2-}\cdot nH_2O$; Calculated binding energies by SAPT2+/aug-cc-pVDZ(-pp) method for the three lowest-lying isomers; 20K NIPE spectra measured with 193 nm (6.424 eV) photons versus 157 nm (7.866 eV). Optimized structures of the three lowest isomers; Numbers of B-X···H-O (solute-solvent) bonds and O···H-O (solvent-solvent) HBs in $B_{12}X_{12}^{2-}\cdot nH_2O$; Plots of the independent gradient model (IGM).

AUTHOR INFORMATION

Corresponding Authors

Haitao Sun − *State Key Laboratory of Precision Spectroscopy, School of Physics and Electronic Science, East China Normal University, Shanghai 200241, China; Collaborative Innovation Center of Extreme Optics, Shanxi University, Taiyuan, Shanxi 030006, China; NYU-ECNU Center for Computational Chemistry at NYU Shanghai, Shanghai, 200062, China;* orcid.org/0000-0003-1471-8876; Email: htsun@phy.ecnu.edu.cn

Xue-Bin Wang − *Physical Sciences Division, Pacific Northwest National Laboratory, Richland, Washington 99352, United States;* orcid.org/0000-0001-8326-1780; Email: xuebin.wang@pnnl.gov

Zhenrong Sun − *State Key Laboratory of Precision Spectroscopy, School of Physics and Electronic Science, East China Normal University, Shanghai 200241, China; Collaborative Innovation Center of Extreme Optics, Shanxi University, Taiyuan, Shanxi 030006, China;* Email: zrsun@phy.ecnu.edu.cn

Authors

Yanrong Jiang − *State Key Laboratory of Precision Spectroscopy, School of Physics and Electronic Science, East China Normal University, Shanghai 200241, China; Center for Transformative Science, ShanghaiTech University,*

Shanghai 201210, China

Zhaojie Cai − *State Key Laboratory of Precision Spectroscopy, School of Physics and Electronic Science, East China Normal University, Shanghai 200241, China*

Qinqin Yuan − *Physical Sciences Division, Pacific Northwest National Laboratory, Richland, Washington 99352, United States*

Wenjin Cao − *Physical Sciences Division, Pacific Northwest National Laboratory, Richland, Washington 99352, United States*

Zhubin Hu − *State Key Laboratory of Precision Spectroscopy, School of Physics and Electronic Science, East China Normal University, Shanghai 200241, China*

Author Contributions

[#]Y.J. and Z.C. contributed equally to this work.

Notes

The authors declare no competing financial interest.

ACKNOWLEDGEMENTS

The work was partly supported by the National Natural Science Foundation of China (No. 12274128, 12034008 and 11727810), Shanghai Rising-Star Program (No. 21QA1402600), and the Program of Introducing Talents of Discipline to Universities 111 Project (B12024). The NIPES work was supported by the U.S. Department of Energy (DOE), Office of Science, Office of Basic Energy Sciences, Division of Chemical Sciences, Geosciences, and Biosciences, and performed using EMSL, a national scientific user facility sponsored by DOE's Office of Biological and Environmental Research and located at Pacific Northwest National Laboratory, which is operated by Battelle Memorial Institute for the DOE. We acknowledge the ECNU Multifunctional Platform for Innovation (001) and HPC Research Computing Team for

providing computational and storage resources.

REFERENCES

(1) Knipping, E. M.; Lakin, M. J.; Foster, K. L.; Jungwirth, P.; Tobias, D. J.; Gerber, R. B.; Dabdub, D.; Finlayson-Pitts, B. J. Experiments and Simulations of Ion-Enhanced Interfacial Chemistry on Aqueous NaCl Aerosols. *Science* **2000**, *288*, 301-306.

(2) Tobias, D. J.; Hemminger, J. C. Getting Specific About Specific Ion Effects. *Science* **2008**, *319*, 1197-1198.

(3) Jungwirth, P.; Tobias, D. J. Specific Ion Effects at the Air/Water Interface. *Chem. Rev.* **2006**, *106*, 1259-1281.

(4) Hribar, B.; Southall, N. T.; Vlachy, V.; Dill, K. A. How Ions Affect the Structure of Water. *J. Am. Chem. Soc.* **2002**, *124*, 12302-12311.

(5) Ma, T.; Easley, A. D.; Wang, S.; Flouda, P.; Lutkenhaus, J. L. Mixed Electron-Ion-Water Transfer in Macromolecular Radicals for Metal-Free Aqueous Batteries. *Cell Rep. Phys. Sci.* **2021**, *2*, 100414.

(6) Barba-Bon, A.; Salluce, G.; Lostalé-Seijo, I.; Assaf, K. I.; Hennig, A.; Montenegro, J.; Nau, W. M. Boron Clusters as Broadband Membrane Carriers. *Nature* **2022**, *603*, 637-642.

(7) Lybrand, T. P.; McCammon, J. A.; Wipff, G. Theoretical Calculation of Relative Binding Affinity in Host-Guest Systems. *Proc. Natl. Acad. Sci.* **1986**, *83*, 833-835.

(8) Chalikian, T. V.; Völker, J.; Plum, G. E.; Breslauer, K. J. A More Unified Picture for the Thermodynamics of Nucleic Acid Duplex Melting: A Characterization by Calorimetric and Volumetric Techniques. *Proc. Natl. Acad. Sci.* **1999**, *96*, 7853-7858.

(9) Kropman, M. F.; Bakker, H. J. Dynamics of Water Molecules in Aqueous Solvation Shells. *Science* **2001**, *291*, 2118-2120.

(10) Habuchi, S.; Kim, H.-B.; Kitamura, N. Water Structures in Ion-Exchange Resin Particles: Solvation Dynamics of Nile Blue A. *Anal. Chem.* **2001**, *73*, 366-372.

(11) Marcus, Y. Effect of Ions on the Structure of Water: Structure Making and Breaking. *Chem. Rev.* **2009**, *109*, 1346-1370.

(12) Collins, K. D. Ions from the Hofmeister Series and Osmolytes: Effects on Proteins in Solution and in the Crystallization Process. *Methods* **2004**, *34*, 300-311.

(13) Zhang, Y.; Cremer, P. S. Interactions between Macromolecules and Ions: the Hofmeister Series. *Curr. Opin. Chem. Biol.* **2006**, *10*, 658-663.

(14) Hyde, A. M.; Zultanski, S. L.; Waldman, J. H.; Zhong, Y.-L.; Shevlin, M.; Peng, F. General Principles and Strategies for Salting-Out Informed by the Hofmeister Series. *Org. Process Res. Dev.* **2017**, *21*, 1355-1370.

(15) Valiev, M.; Deng, S. H. M.; Wang, X.-B. How Anion Chaotrope Changes the Local Structure of Water: Insights from Photoelectron Spectroscopy and Theoretical Modeling of SCN^- Water Clusters. *J. Phys. Chem. B* **2016**, *120*, 1518-1525.

(16) Baer, M. D.; Pham, V.-T.; Fulton, J. L.; Schenter, G. K.; Balasubramanian, M.; Mundy, C. J. Is Iodate a Strongly Hydrated Cation? *J. Phys. Chem. Lett.* **2011**, *2*, 2650-2654.

(17) Venkateshwaran, V.; Vembanur, S.; Garde, S. Water-Mediated Ion-Ion Interactions are Enhanced at the Water Vapor-Liquid Interface. *Proc. Natl. Acad. Sci.*

2014, *111*, 8729-8734.

(18) Biedermann, F.; Nau, W. M.; Schneider, H.-J. The Hydrophobic Effect Revisited—Studies with Supramolecular Complexes Imply High-Energy Water as a Noncovalent Driving Force. *Angew. Chem. Int. Ed.* **2014**, *53*, 11158-11171.

(19) Assaf, K. I.; Nau, W. M. The Chaotropic Effect as An Assembly Motif in Chemistry. *Angew. Chem. Int. Ed.* **2018**, *57*, 13968-13981.

(20) Verlet, J. R. R.; Bragg, A. E.; Kammrath, A.; Cheshnovsky, O.; Neumark, D. M. Observation of Large Water-Cluster Anions with Surface-Bound Excess Electrons. *Science* **2005**, *307*, 93-96.

(21) Jian, F. F.; Liu, E.; Ma, J. Y. Interesting fluorine anion water clusters $[F^{-}\cdot(H_2O)_n]$ in metal complex crystals. *CrystEngComm* **2018**, *20*, 3849-3857.

(22) Liu, J.; Yang, J.; Zeng, X. C.; Xantheas, S. S.; Yagi, K.; He, X. Towards Complete Assignment of The Infrared Spectrum of the Potonated Wter Custer $H^{+}(H_2O)_{21}$. *Nat. Commun.* **2021**, *12*, 6141.

(23) Zhang, B.; et al. Infrared Spectroscopy of Neutral Water Clusters at Finite Temperature: Evidence for A Noncyclic Pentamer. *Proc. Natl. Acad. Sci.* **2020**, *117*, 15423-15428.

(24) Gruenloh, C. J.; Carney, J. R.; Arrington, C. A.; Zwier, T. S.; Fredericks, S. Y.; Jordan, K. D. Infrared Spectrum of a Molecular Ice Cube: The S_4 and D_{2d} Water Octamers in Benzene-$(Water)_8$. *Science* **1997**, *276*, 1678-1681.

(25) Robertson, W. H.; Diken, E. G.; Price, E. A.; Shin, J.-W.; Johnson, M. A. Spectroscopic Determination of the OH^{-} Solvation Shell in the $OH^{-}\cdot(H_2O)_n$ Clusters. *Science* **2003**, *299*, 1367-1372.

(26) Bragg, A. E.; Verlet, J. R. R.; Kammrath, A.; Cheshnovsky, O.; Neumark, D. M. Hydrated Electron Dynamics: From Clusters to Bulk. *Science* **2004**, *306*, 669-671.

(27) Nauta, K.; Miller, R. E. Formation of Cyclic Water Hexamer in Liquid Helium: The Smallest Piece of Ice. *Science* **2000**, *287*, 293-295.

(28) Li, G.; et al. Infrared Spectroscopic Study of Hydrogen Bonding Topologies in the Smallest Ice Cube. *Nat. Commun.* **2020**, *11*, 5449.

(29) Ludwig, R. Water: From Clusters to the Bulk. *Angew. Chem. Int. Ed.* **2001**, *40*, 1808-1827.

(30) Aprà, E.; Warneke, J.; Xantheas, S. S.; Wang, X.-B. A Benchmark Photoelectron Spectroscopic and Theoretical Study of the Electronic Stability of $[B_{12}H_{12}]^{2-}$. *J. Chem. Phys.* **2019**, *150*, 164306.

(31) Warneke, J.; Hou, G.-L.; Aprà, E.; Jenne, C.; Yang, Z.; Qin, Z.; Kowalski, K.; Wang, X.-B.; Xantheas, S. S. Electronic Structure and Stability of $[B_{12}X_{12}]^{2-}$ (X = F–At): A Combined Photoelectron Spectroscopic and Theoretical Study. *J. Am. Chem. Soc.* **2017**, *139*, 14749-14756.

(32) Warneke, J.; Jenne, C.; Bernarding, J.; Azov, V. A.; Plaumann, M. Evidence for An Intrinsic Binding Force between Dodecaborate Dianions and Receptors with Hydrophobic Binding Pockets. *Chem. Commun.* **2016**, *52*, 6300-6303.

(33) Assaf, K. I.; Ural, M. S.; Pan, F.; Georgiev, T.; Simova, S.; Rissanen, K.; Gabel, D.; Nau, W. M. Water Structure Recovery in Chaotropic Anion Recognition: High-Affinity Binding of Dodecaborate Clusters to γ-Cyclodextrin. *Angew. Chem. Int. Ed.*

2015, *54*, 6852-6856.

(34) Cígler, P.; et al. From Nonpeptide toward Noncarbon Protease Inhibitors: Metallacarboranes as Specific and Potent Inhibitors of HIV Protease. *Proc. Natl. Acad. Sci.* **2005**, *102*, 15394-15399.

(35) Karki, K.; Gabel, D.; Roccatano, D. Structure and Dynamics of Dodecaborate Clusters in Water. *Inorg. Chem.* **2012**, *51*, 4894-4896.

(36) Jiang, Y.; et al. Unraveling Hydridic-to-Protonic Dihydrogen Bond Predominance in Monohydrated Dodecaborate Clusters. *Chem. Sci.* **2022**, *13*, 9855-9860.

(37) Teeter, M. M. Water Structure of A Hydrophobic Protein at Atomic Resolution: Pentagon Rings of Water MMolecules in Crystals of Crambin. *Proc. Natl. Acad. Sci.* **1984**, *81*, 6014-6018.

(38) Neidle, S.; Berman, H. M.; Shieh, H. S. Highly Structured Water Network in Crystals of A Deoxydinucleoside–Drug Complex. *Nature* **1980**, *288*, 129-133.

(39) Jiang, Y.; et al. Gaseous Cyclodextrin-Closo-Dodecaborate Complexes $\chi CD{\cdot}B_{12}X_{12}^{2-}$ (χ = α, β, and γ; X = F, Cl, Br, and I): Electronic Structures and Intramolecular Interactions. *Phys. Chem. Chem. Phys.* **2021**, *23*, 13447-13457.

(40) Li, Z.; Jiang, Y.; Yuan, Q.; Warneke, J.; Hu, Z.; Yang, Y.; Sun, H.; Sun, Z.; Wang, X. B. Photoelectron Spectroscopy and Computational Investigations of the Electronic Structures and Noncovalent Interactions of Cyclodextrin-Closo-Dodecaborate Anion Complexes χ-CD.$B_{12}X_{12}^{2-}$ (χ = α, β, and γ; X = H, F). *Phys. Chem. Chem. Phys.* **2020**, *22*, 7193-7200.

(41) Wang, X.-B.; Wang, L.-S. Development of A Low-Temperature Photoelectron Spectroscopy Instrument using An Electrospray Ion Source and A Cryogenically Controlled Ion Trap. *Rev. Sci. Instrum.* **2008**, *79*, 073108.

(42) Lu, T. *Molclus Program*, Beijing Kein Research Center for Natural Science: 2016.

(43) Bannwarth, C.; Ehlert, S.; Grimme, S. GFN2-xTB—An Accurate and Broadly Parametrized Self-Consistent Tight-Binding Quantum Chemical Method with Multipole Electrostatics and Density-Dependent Dispersion Contributions. *J. Chem. Theory Comput.* **2019**, *15*, 1652-1671.

(44) Bursch, M.; Neugebauer, H.; Grimme, S. Structure Optimisation of Large Transition-Metal Complexes with Extended Tight-Binding Methods. *Angew. Chem. Int. Ed.* **2019**, *58*, 11078-11087.

(45) Adamo, C.; Barone, V. Toward Reliable Density Functional Methods without Adjustable Parameters: The PBE0 model. *J. Chem. Phys.* **1999**, *110*, 6158-6170.

(46) Weigend, F.; Ahlrichs, R. Balanced Basis Sets of Split Valence, Triple Zeta Valence and Quadruple Zeta Valence Quality for H to Rn: Design and Assessment of Accuracy. *Phys. Chem. Chem. Phys.* **2005**, *7*, 3297-3305.

(47) Kendall, R. A.; Dunning, T. H.; Harrison, R. J. Electron Affinities of the First-Row Atoms Revisited. Systematic Basis Sets and Wave Functions. *J. Chem. Phys.* **1992**, *96*, 6796-6806.

(48) Peterson, K. A.; Shepler, B. C.; Figgen, D.; Stoll, H. On the Spectroscopic and Thermochemical Properties of ClO, BrO, IO, and Their Anions. *J. Phys. Chem. A* **2006**,

110, 13877-13883.

(49) Grimme, S.; Antony, J.; Ehrlich, S.; Krieg, H. A Consistent and Accurate ab initio Parametrization of Density Functional Dispersion Correction (DFT-D) for the 94 Elements H-Pu. *J. Chem. Phys.* **2010**, *132*, 154104.

(50) Grimme, S.; Ehrlich, S.; Goerigk, L. Effect of the Damping Function in Dispersion Corrected Density Functional Theory. *J. Comput. Chem.* **2011**, *32*, 1456-1465.

(51) Riplinger, C.; Sandhoefer, B.; Hansen, A.; Neese, F. Natural Triple Excitations in Local Coupled Cluster Calculations with Pair Natural Orbitals. *J. Chem. Phys.* **2013**, *139*, 134101.

(52) Neese, F.; Wennmohs, F.; Hansen, A. Efficient and Accurate Local Approximations to Coupled-Electron Pair Approaches: An Attempt to Revive the Pair Natural Orbital Method. *J. Chem. Phys.* **2009**, *130*, 114108.

(53) Neese, F. Software update: the ORCA program system, version 4.0. *WIREs Comput. Mol. Sci.* **2018**, *8*, e1327.

(54) Merrick, J. P.; Moran, D.; Radom, L. An Evaluation of Harmonic Vibrational Frequency Scale Factors. *J. Phys. Chem. A* **2007**, *111 45*, 11683-700.

(55) Hohenstein, E. G.; Sherrill, C. D. Density Fitting of Intramonomer Correlation Effects in Symmetry-Adapted Perturbation Theory. *J. Chem. Phys.* **2010**, *133*, 014101.

(56) Parker, T. M.; Burns, L. A.; Parrish, R. M.; Ryno, A. G.; Sherrill, C. D. Levels of Symmetry Adapted Perturbation Theory (SAPT). I. Efficiency and Performance for Interaction Energies. *J. Chem. Phys.* **2014**, *140*, 094106.

(57) Parrish, R. M.; et al. Psi4 1.1: An Open-Source Electronic Structure Program Emphasizing Automation, Advanced Libraries, and Interoperability. *J. Chem. Theory Comput.* **2017**, *13*, 3185-3197.

(58) Frisch, M. J.; et al. *Gaussian 16 Rev. A.03*, Wallingford, CT, 2016.